Check for updates

Original Research Article

Applied Spectroscopy Practica
2025, Vol. 3(1) 1–12
© The Author(s) 2025
Article reuse guidelines:
sagepub.com/journals-permissions
DOI: 10.1177/27551857251327408
journals.sagepub.com/home/app
Sage

Diagenetic Processes in the Fossilized Carapace of *Neosclerocalyptus* sp. from the Paraguayan Chaco

Deyne SM Buzarquis Arias[1], Edher Herrera[1,2], Christian F Colman[1], Yennifer Sarubbi Jacks[1], Sergio D Ríos[3], Ricardo Souberlich[1], Christian J Sánchez Gonzales[1,4], and Alex Matos da Silva Costa[1]

Abstract

Paleometry is essential in analyzing fossil remains, revealing diagenetic processes through physicochemical characterization techniques that identify crystalline and chemical structures, as well as elemental composition and changes observed via electron microscopy. This study examines the fossilized carapace of *Neosclerocalyptus* sp. from the Paraguayan Chaco, employing these methodologies to understand its diagenetic transformation. Fourier transform infrared (FT-IR) spectra identified phosphate, carbonate, and amide I and II groups. The Gaussian deconvolution model applied to the FT-IR spectra distinguished individual bands within overlapping vibrational modes, providing insights into the presence of stoichiometric and non-stoichiometric calcium phosphates. X-ray diffraction patterns confirmed the crystallinity and apatite nature of the sample, while energy dispersive X-ray fluorescence and scanning electron microscopy energy-dispersive spectroscopy assessed its elemental composition and microstructural characteristics. The results indicated the inclusion of new crystalline phases (quartz) and changes in mineralogy and crystallinity due to environmental interactions. A diagenetic pathway model is proposed, involving initial development, exposure to calcium carbonate-rich water, hydroxyapatite recrystallization, calcite infiltration in pores, and incorporation of new elements. This study enhances the understanding of fossil preservation and environmental influences on diagenetic processes at a regional level as well as being one of the first works on glyptodont carapace characterizations in South America.

Keywords

Diagenesis process, *Neosclerocalyptus* sp., hydroxyapatite, spectroscopic analysis, Fourier transform infrared, FT-IR, X-ray fluorescence, XRF, X-ray diffraction, XRD, scanning electron microscopy energy-dispersive spectroscopy, SEM-XRD, paleometry

Date received: 2 September 2024; accepted: 27 January 2025

Introduction

Paleometry is crucial for understanding fossil remains, integrating geology, biology, chemistry, and physics to reveal the origins and evolution of life on Earth and beyond.[1,2] Using techniques such as spectroscopy, it preserves rare fossils while deducing how they and their surrounding sediments change over time.[1,3–5] Paleometry helps reconstruct ancient ecosystems, providing insights into past climates, habitats, and biodiversity, which are key to interpreting evolutionary processes. It also clarifies how environmental factors affect fossil preservation, ensuring a more accurate interpretation of the fossil record.[2,6] Techniques such as Fourier transform infrared (FT-IR) spectroscopy, X-ray diffraction (XRD), X-ray fluorescence (XRF) spectrometry, and scanning electron microscopy energy-dispersive spectroscopy (SEM-EDS) are integral to this research. These advanced methodologies facilitate in-depth molecular-level analyses of fossils and their environmental interactions, providing critical insights into their formation and preservation. Specifically, the rapid

[1]Facultad de Ciencias Exactas y Naturales, FACEN–UNA, San Lorenzo, Paraguay
[2]Department of Condensed Matter, Applied Physics and Nanoscience, Brazilian Center for Research in Physics, Rio de Janeiro, Brazil
[3]Departamento de Arqueología y Paleontología, Secretaría Nacional de Cultura, Asunción, Paraguay
[4]Comisión Nacional de Energía Atómica—Dirección General de Investigación Científica y Tecnológica—Universidad Nacional de Asunción, San Lorenzo, Paraguay

Corresponding Author:
Alex Matos da Silva Costa, Facultad de Ciencias Exactas y Naturales, FACEN–UNA, Campus/UNA, Km 11, C.C. 1039–1804, San Lorenzo, Paraguay.
Email: alexmatos@facen.una.py

Creative Commons Non Commercial CC BY-NC: This article is distributed under the terms of the Creative Commons Attribution-NonCommercial 4.0 License (https://creativecommons.org/licenses/by-nc/4.0/) which permits non-commercial use, reproduction and distribution of the work without further permission provided the original work is attributed as specified on the SAGE and Open Access page (https://us.sagepub.com/en-us/nam/open-access-at-sage).

identification of phosphate groups associated with apatite materials uncovers the complex interplay between groundwater chemistry and diagenetic transformations in biogenic materials.[1,3–5,7,8]

When analyzing bones, the primary focus is on apatite, predominantly in the form of calcium phosphate, which serves as the principal inorganic component of bone, vertebrate teeth, and certain carapaces or shells.[9,10] Bone mineral composition is approximately 60–70% inorganic material, mainly hydroxyapatite ($Ca_{10}(PO_4)_6(OH)_2$), which provides structural rigidity and strength.[11] The remaining 25% consists of organic material, largely type I collagen, along with non-collagenous proteins and lipids. Besides hydroxyapatite, the inorganic phase contains minor calcium phosphates such as brushite and tricalcium phosphate, as well as trace elements like magnesium and sodium, which can substitute for calcium within the hydroxyapatite lattice.[7]

Natural variations in bone composition can arise from factors such as diet and metabolism, leading to ionic substitutions at both calcium and phosphate sites. In contrast, changes during fossilization are indicated by the presence of increased carbonate ions, which can substitute for phosphate in the apatite structure, as well as alterations in crystallinity and the introduction of foreign minerals due to groundwater infiltration.[2,11] These substitutions create atomic-level disruptions that can notably alter the physical properties of bone crystals following burial.[12–14]

These changes involve the degradation of the bone's organic matrix by microorganisms, happening both before and during transport and sedimentary events, recrystallization and ion absorption. Subsequent processes after deposition depend on site conditions such as the mineralogical composition of the sediment, pH, temperature, and water characteristics.[2,9,15,16]

The diagenesis process encompasses the physical and chemical transformations that carbonate hydroxyapatite experiences in sediments due to groundwater exposure. Key processes include dissolution and recrystallization, where minerals are leached and then re-precipitated into more stable forms, as well as crystal growth, which alters structural integrity without necessarily dissolving the original material.[2,7,17,18]

In 2020, a carapace of a *Neosclerocalyptus* sp. was collected outside Neuland, Boquerón Department, near the center of the Paraguayan Chaco. This study focuses on conducting a rigorous characterization of the fossil remain. A potential model of diagenetic pathways was proposed based on the geological conditions surrounding the fossil as well as its alterations.

We hypothesize that the partial preservation of organic materials within the osteoderms may have been influenced either by an early interruption in the fossilization process or by more recent contamination. This preservation might have been facilitated by the osteoderms' isolation and protection within an inorganic matrix, where cementation occurred, preventing complete permineralization. Alternatively, it may result from the deposition of organic material from the surrounding environment.[19,20]

Geological Environment

The Cenozoic sedimentary system which occurs in the central portion of South America, known as Chaco, spans around 840 000 km^2 and extends from the Sub-Andean Sierras to the Paraná basin, covering parts of northeastern Argentina, southern Bolivia and western Paraguay. Shaped by six major river systems, including the Pilcomayo and Bermejo rivers, which flow eastward from the Andes towards the Paraguay and Paraná rivers, the region is characterized by large alluvial fans, creating a landscape of ancient channels, meandering lakes, and swampy areas.[21–33] It is essential to understand the sedimentary context of the Paraguayan Chaco, a region whose geological evolution reveals that it is largely composed of transported soils, ranging from sandy loam to clay.[34]

Sedimentation in the Chaco began in the Oligocene period and continues to this day. These sediments, carried from the Andes, have deposited thick layers across the plains, shaped by two key phases of river activity: one during the late Pleistocene and another after the Ice Age.[21–24,35] Wet climates stabilized the river systems, leading to finer sediment deposits, while dry periods led channels to shift and increased sedimentation. Evidence of old riverbeds are still visible, especially in the Pilcomayo system, one of the most sediment-rich rivers in the world, transporting around 140 million tons of sediment annually.[24,28]

Fossil remains of *Neosclerocalyptus* sp. were found about 3 m deep in Neuland, a part of the Boquerón District, seen in Figure 1a. This place is within the central area of the Pilcomayo River's alluvial fan that spans over 210 000 km^2 and extends more than 1000 km from its starting point to the Paraguay River.[24,28] The region's depositional environments have evolved: it began with short-lived braided streams and hardened soils in the late Oligocene, transitioning to large riverbanks that created thick deposits on the floodplain, pushing sediment progressively eastward.[23]

The Chaco's geological history has a significant impact on bone preservation. As sediments accumulate, minerals can leach into buried bones, altering their chemical composition and potentially modifying isotopic ratios. Climatic fluctuations, alternating between wet and dry periods, further influence sedimentation, which directly affects bone chemistry. During diagenesis, interactions like groundwater movement through sediments can further modify the bones. In the Chaco, where river activity drives significant sediment transport, these processes are particularly important to consider during fossil analysis.[22,34,36]

Experimental

Materials and Methods

The carapace presented in this manuscript was discovered and collected in September 2020 from the plains near Neuland

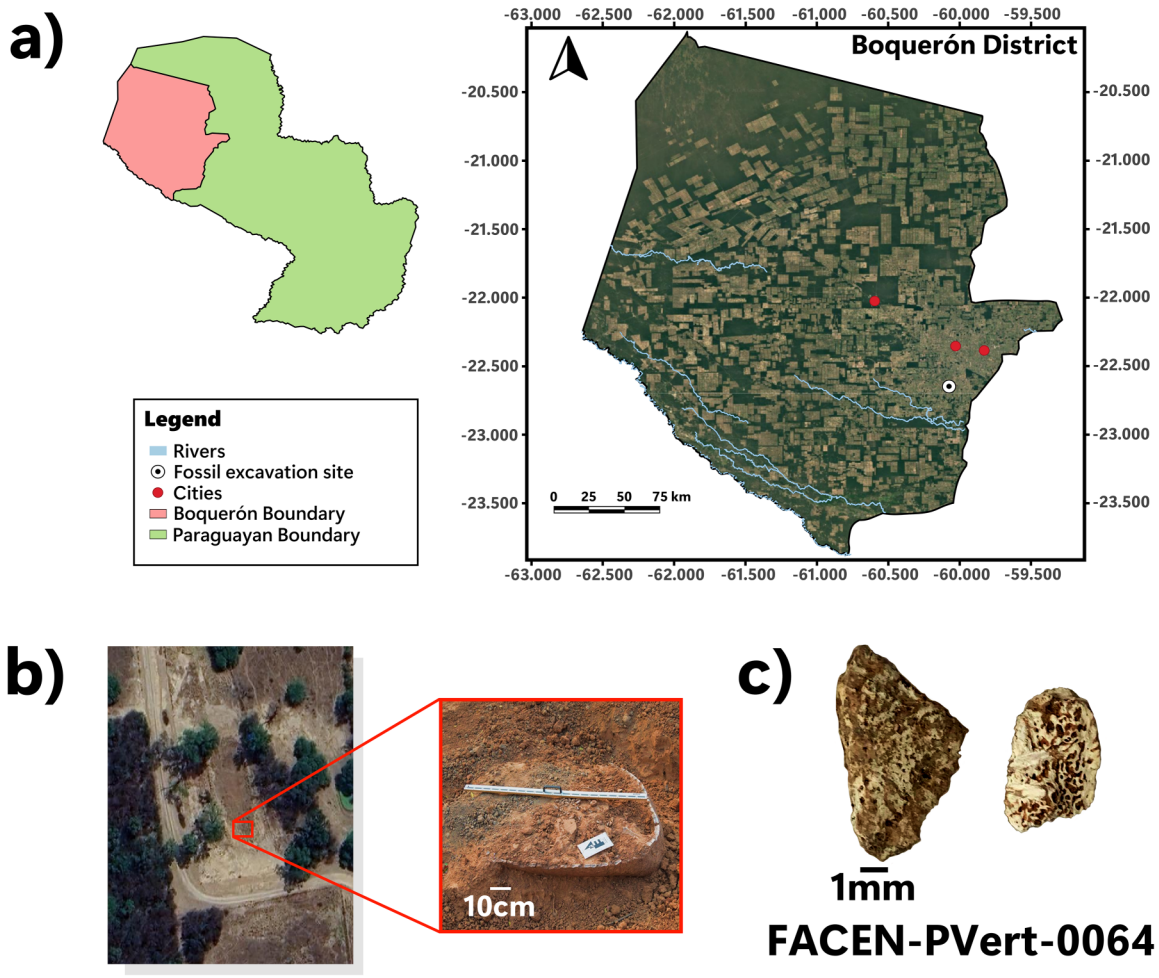

Figure 1. (a) Location map of the glyptodont's carapace fossil discovery site. (b) Excavation site of the fossil carapace. (c) Analyzed fragments of the glyptodont's carapace fossil of *Neosclerocalyptus* sp., coded as FACEN-PVert-0064.

Town (latitude: 22°38′53.61'S; longitude: 60°4′38.77″W), in the Boquerón Department of Western Paraguay,[37] as seen in Figure 1b. The partial carapace is deposited at the Laboratorio de Paleontología, Facultad de Ciencias Exactas y Naturales, Universidad Nacional de Asunción, under the collection number FACEN-PVert-0064.

The fossil remains were assigned to the genus *Neosclerocalyptus* based on certain diagnostic characteristics, including a reduced size compared to other taxa, a low and elongated subcylindrical dorsal carapace, and elongated rectangular lateral plates that are relatively thin with a central figure larger than the peripheral ones.[38,39] Although the genus *Neosclerocalyptus* is represented by five recognized species: *N. castellanosi*, *N. ornatus*, *N. pseudornatus*, *N. gouldi*, and *N. paskoensis*,[40] one of the diagnostic features for species assignment is the development and pneumatization of the frontonasal sinuses, as well as their extensively studied and recognized biostratigraphical distribution.[41]

Nevertheless, the absence of the skull and other diagnostic aspects of the skeleton, along with the uncertainty about the age of the sediments in which the specimen was found, prevent us from assigning the materials to one of the recognized species of the *Neosclerocalyptus* genera.

Two small peripheric osteoderm fragments from the edge of the dorsal carapace were selected for this study, presented in Figure 1c. These fragments were chosen due to their relatively protected location, being less exposed to surrounding sediments. After careful cleaning, the samples were placed in sterile bags to prevent any contamination, either during field collection or later in the laboratory.

FT-IR spectroscopy measurements were conducted using an IRAffinity-1 Infrared Spectrometer (Shimadzu) configured with a spectral resolution of 0.5 cm^{-1} and set to 4 cm^{-1}. The instrument performed 128 scans over a spectral range of 400 to 4000 cm^{-1}. The sample preparation involved pulverizing a small fragment of the fossil with a mortar and pestle, followed by the addition of potassium bromide (KBr) powder as a binding agent. The mixture was then pressed to form a pellet, which was then measured in transmission mode.

For spectral processing, the FT-IR spectra underwent baseline corrections, smoothing, and second derivative calculations,[42,43] performed three times using the Spectragryph software.[44] Among the three collected FT-IR spectra, the most representative one was selected for detailed analysis. The deconvolution of IR spectra utilized a model of N coupled Gaussian oscillators adopted for calcium phosphates,[45–47] identifying regions of interest (ROI) where these compounds exhibited a response. The second derivative of the spectra was calculated to locate the minima. Deconvolution was carried out using the Gaussian deconvolution model (GDM) via the open-source software Fityk,[48] where each curve's centroid corresponds to an active band, and intensity relates to the number of oscillators, considering common active modes in IR and the second derivative minima.[49]

The XRD analyses were performed using a PANalytical X'Pert Pro MRD diffractometer (Malvern Panalytical), featuring a spectral resolution of approximately 5 arcseconds.[3] The analysis employed a Cu Kα radiation source with a wavelength of $\lambda = 1.54060$ Å and a powdered FACEN-PVert-0064 sample. The angular measurement range spanned from 5° to 60° at a step size of 0.025 degrees and an accumulation time of 3 seconds for each angular position, aiming to optimize the signal-to-noise ratio. The analysis involved comparing the crystalline phase pattern with the experimental X-ray diffractogram.

The elemental composition of FACEN-PVert-0064 was qualitatively assessed using the EDX-7000 energy dispersive X-ray fluorescence system (Shimadzu), achieving an energy resolution of less than 140 eV for the Mn Kα line, equipped with a Rh anode and a solid-state-type detector. All EDXRF spectra analyses were done using the PCEDX Pro software by fundamentals parameters methods for semiquantitative analysis.

The microstructure was examined through scanning electron microscopy (SEM). Prior to the SEM analysis, the fossil remains underwent a standardized carbon-coating process to mitigate electron accumulation effects on irregular surfaces, executed at a 4 V for 8 seconds of carbon deposition time. The samples were subsequently examined using secondary electron imaging with a CX-200 Plus scanning electron microscope (COXEM Co., Ltd.), which boasts a spectral resolution of less than 3 nm at an acceleration voltage of 30 kV. For this study, however, the SEM operated at a voltage of 20 kV to optimize imaging conditions.

Finally, for enhanced characterization, a specific zone of the sample was subjected to elemental mapping with an energy dispersive X-ray spectrometer (EDS) equipped with an EDS Xplore30 Detector (Oxford Instruments), noted for its spectral resolution of approximately 129 eV for the Mn Kα peak at a count rate of 100 000 counts per second.

To ensure a comprehensive characterization, sediment samples were collected from an area in proximity to the fossil fragments. These sediments underwent the same analytical procedures, including FT-IR, XRD, EDXRF, and SEM-EDS analyses (Supplemental Material), thus maintaining consistency in the evaluation process.

Results

The FT-IR analysis revealed key functional groups characteristic of apatitic structures, including phosphates (PO_4^{3-}), carbonates (CO_3^{2-}), hydroxyl (OH^-), and organic components. Figure 2a illustrates the specific absorption bands, while Table 1 details these spectral features, following a conventional FT-IR analysis approach for fossil samples. Phosphate groups exhibited O–P–O bond bending modes, and P–O bonds showed symmetric and asymmetric stretching modes.[42,45,50–59] A potential vibrational signal for hydrogen phosphate (HPO_4^{2-}) was also noted.[50]

Table 1 further identifies the carbonate group, indicating possible ionic substitutions within the apatitic structure.[45,50,56,60] Additionally, the amide I group and overlapped

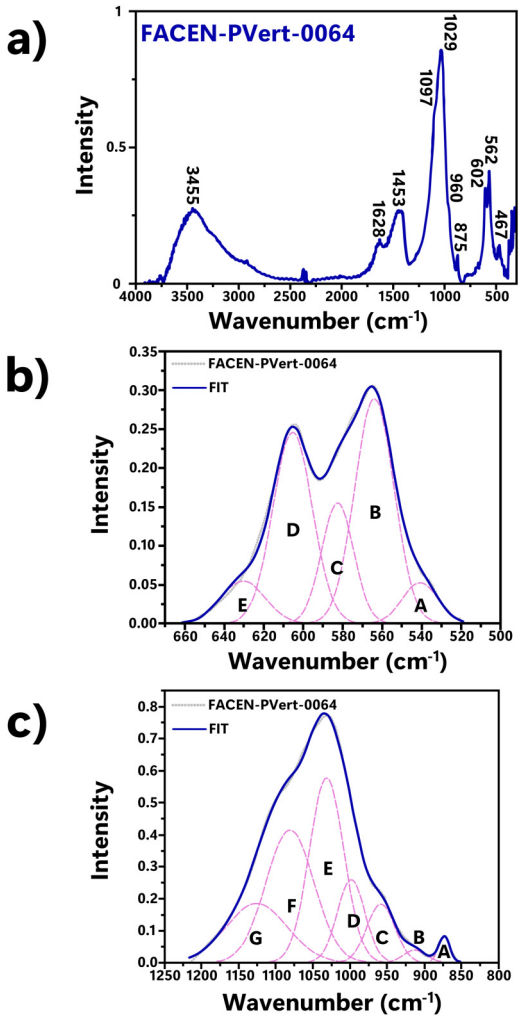

Figure 2. (a) FT-IR spectra of FACEN-PVert-0064. (b) Gaussian deconvolution of the ROI (700–400 cm^{-1}). (c) Gaussian deconvolution of the ROI (1300–800 cm^{-1}).

Table I. Assigned bands from the FT-IR spectrum of FACEN-PVert-0064.

Wavenumber (cm^{-1})	Assignation	References
467	Double degenerated bending mode (ν_2) of the phosphate group PO_4 (O–P–O bond)	50,56,59
562	Triply degenerated bending mode (ν_4) of the phosphate group PO_4 (O–P–O bond)	45,50,56–58
602	Triply degenerated bending mode (ν_4) of the phosphate group PO_4 (O–P–O bond)	45,50,56,58
875	Characteristic peak of hydrogen phosphate group (nondistinguishable peak) or a possible bending mode (ν_4 or ν_3) of carbonate group CO_3 in carbonated apatites	45,50,56,60
960	Nondegenerated symmetric stretching mode (ν_1) of the phosphate group PO_4 (P–O bond)	50–52
1029	Triply degenerated asymmetric stretching mode (ν_3) of the phosphate group PO_4 (P–O bond)	42,54,58
1097	Triply degenerated asymmetric stretching mode (ν_3) of the phosphate group PO_4 (P–O bond)	53,55
1453	Amide II or a doublet band (ν_3) of the carbonate group CO_3	19,53,61
1628	Amide I (β-sheets) or a possible adsorbed water band	45,52,61–63
3455	Stretching mode (ν_s) of the hydroxyl group OH or a possible adsorbed water band	53,54,63,64

signals from adsorbed water on clay were observed,[45,52,61–63] along with stretching modes of hydroxyl groups and a broad peak attributed to adsorbed water.[53,54,63,64] Finally, the amide II group or a doublet band (ν_3) of the carbonate group was detected.[19,53,61]

Given the broad FT-IR spectrum, it is crucial to focus on the overlapping bands in the ranges of 700–400 cm^{-1} and 1300–800 cm^{-1}, as they reveal multiple absorption bands related to carbonate ionic substitutions and phosphate groups. Although these overlaps complicate precise identification, this complexity is effectively addressed through the deconvolutions shown in Figure 2b and 2c, and summarized in Tables II and III.

Table II presents the deconvolution of the first ROI from 700 to 400 cm^{-1}, where the phosphate group exhibits O–P–O bond bending modes and triply degenerated bending modes (ν_4).[45,50,58,65] Additionally, a librational mode (ν_L) of the hydroxyl group is observed at 630.45 cm^{-1}.[50]

In the ROI of 1300–800 cm^{-1}, detailed in Table III, several P–O bond vibrational modes of the phosphate group are identified, include a stretching mode (ν_1), a non-degenerate symmetric stretching mode (ν_1), and a triply degenerate asymmetric stretching mode (ν_3). The PO_4 in an apatitic environment appears at 998.484 cm^{-1}, while a band at 1125.63 cm^{-1} is attributed to the presence of hydrogen phosphate.[50,55,58,66] Additionally, a non-apatitic stretching mode (ν_2) of the carbonate group is detected at 873.225 cm^{-1}.[45]

Figure 3a presents the XRD results for FACEN-PVert-0064, confirming the apatitic nature of the sample. The analysis identifies common crystalline phases, including hydroxyapatite, which is prevalent in fossil structures, along with quartz (a silicate) and illite phases. In terms of elemental composition, the XRF results indicate the presence of Ca, P, and Si, consistent with the crystalline phases identified in the XRD analysis, as well as other secondary elements. Additionally, the Kα and Kβ emission lines for Mn and Cr are relatively close in energy, leading to overlapping peaks in the XRF spectrum. This overlap complicates the distinction between these elements, as illustrated in Figure 3b.

The EDXRF results show in Table IV a predominant presence of Si at 41.37% by weight (%wt). Ca and P were also detected, with a Ca/P ratio of approximately 1.72,[50,67] a value close to that of stoichiometric apatites. This ratio is comparable to those found in living organisms, highlighting the preservation of the original chemical composition throughout the fossilization process. Additionally, Al and Fe were identified at 16.032% and 4.739 %wt, respectively, along with 1.234% of traces of Ti, Mn, Sr, Cu, Zn, Cr, Rb, and Ni.

The FACEN-PVert-0064 SEM-EDS results are shown in Figure 4. In Figure 4a, a magenta outline highlighting the zone of interest, accompanied with its magnified SEM image in Figure 4b. EDS results are shown in Figure 4c. The elemental mapping reveals a uniform distribution of constituent elements, particularly notable on the main surface characterized by high porosity and voids.[68] The chemical composition in this area includes Ca, Si, P, Al, Fe, and K.

Discussion

The FT-IR analysis reveals that the apatitic structure of bones contains carbonate ions, which partially overlap with phosphate ions. The deviations observed in the phosphate group bands are correlated with the presence of carbonate ions.[69,70] When comparing the experimental bands to those assigned in the literature, noticeable deviations were observed. The symmetric stretching of the PO_4^{3-} group is particularly sensitive to ionic impurities, especially substitution by CO_3^{2-}. Any alterations in its ionic constituents can significantly affect the characteristics of the band.

Moreover, changes in the full width half-maximum (FWHM) parameters of the performed GDM curves were noted, with values being relatively higher than those reported

Table II. FT-IR band assignments of the GDM from the ROI, 700–400 cm^{-1}.

Band	Center	Area	Full width half-maximum (FWHM)	Assignation	References
A	540.78	1.19225	21.1635	Bending modes of the phosphate group PO_4 (O–P–O bond)	65
B	563.883	7.20892	23.3731	Triply degenerated bending modes (ν_4) of the phosphate group PO_4 (O–P–O bond)	45,50,58
C	582.437	3.16674	19.1294	Triply degenerated bending modes (ν_4) of the phosphate group PO_4 (O–P–O bond)	45,50,58
D	605.257	6.188	23.6065	Triply degenerated bending modes (ν_4) of the phosphate group PO_4 (O–P–O bond)	45,50,58
E	630.45	1.54041	26.357	Librational mode (ν_L) of the hydroxyl group	50

Table III. FT-IR band assignments of the GDM from the ROI, 1300 to 800 cm^{-1}.

Band	Center	Area	FWHM	Assignation	References
A	873.225	1.58788	18.3809	Non-apatitic stretching mode (ν_2) of the carbonate group CO_3	45
B	912.806	1.58248	37.1082	Stretching mode (ν_1) of the phosphate group PO_4	55
C	958.498	8.75716	44.8985	Non-degenerate symmetric stretching mode (ν_1) of the phosphate PO_4 (P–O bond)	50,66
D	998.484	12.1656	43.9676	PO_4 in an apatitic environment	66
E	1031.53	33.764	54.9225	Triply degenerate asymmetric stretching mode (ν_3) of the phosphate PO_4 (P–O bond)	50,58
F	1080.91	33.6672	76.2595	Triply degenerate asymmetric stretching mode (ν_3) of the phosphate PO_4 (P–O bond)	50
G	1125.63	19.1723	97.2591	Due to the presence of HPO_4	66

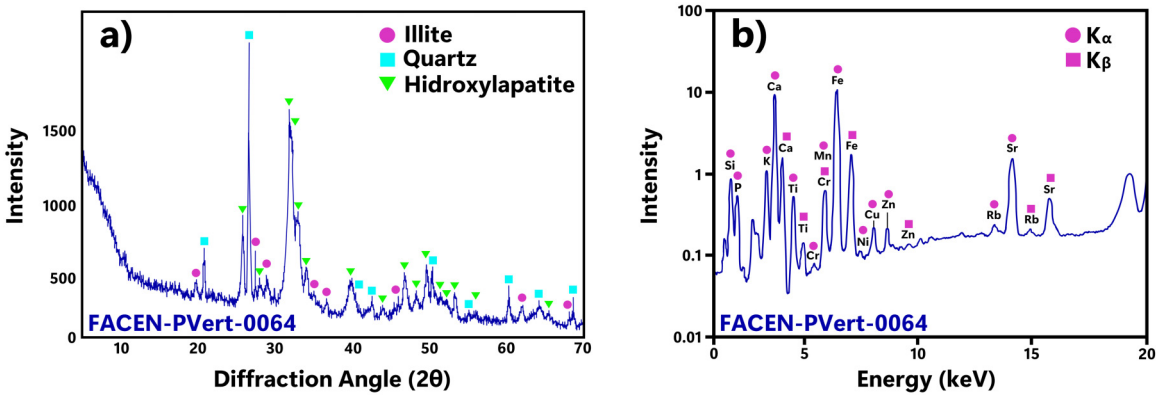

Figure 3. (a) X-ray diffractogram and (b) EDXRF spectrum of FACEN-PVert-0064.

for synthetic hydroxyapatites. This observation aligns with the inversely proportional relationship between FWHM values and their crystallite size; a narrower FWHM indicates higher crystallinity, while broader peaks suggest an increase in amorphous content.[2]

Considering the XRD pattern, it confirms the apatitic nature of the material and indicates the presence of silicates. The phase similar to hydroxyapatite is the most abundant, accompanied by quartz and illite. The crystallinity of illite is a crucial indicator of metamorphic grade in clay-rich rocks that have transformed between diagenesis and low-grade metamorphism,[71] which coincides with the soil condition of the Paraguayan Chaco.[72] In the EDXRF analysis, for the elemental composition, prominent peaks of phosphorus and calcium are visible, which makes sense considering the apatitic structure of bones. The silicon peak is also noteworthy, emphasizing the quartz phase found in the XRD analysis.

Trace elements like Sr, Cu, Zn, and Ni accumulate in bones, reflecting possible environmental conditions and diet during life. Metals such as Mn and Zn are influenced by

both environmental factors and postmortem chemical changes.[73,74] After burial, bones undergo chemical changes, increasing metal concentrations like Mn and Ni through sediment interactions.[73] On the other hand, sediment concentration of Mn, Cr, Ti, Cu, Zn, and Rb vary by location and environmental conditions, often impacted by human activities or natural geological processes.[74–76]

Table IV. Estimation of the percentage weight composition of FACEN-PVert-0064 using the fundamental parameter method in EDXRF.

Element	Result (%wt)	Standard error (3σ)	Intensity
Si	41.37	0.128	2.9672
Ca	20.927	0.023	25.1892
Al	16.032	0.137	0.2544
P	12.128	0.049	1.3526
Fe	4.739	0.007	97.3695
K	3.57	0.01	2.9936
Traces	1.234		

The high percentage of Si, along with the trace elements could be due to the inclusion, surface deposition, and penetration through the pores of the fossil material, originating from the sediment (Figure S1, Figure S2, and Table S1, Supplemental Material) incorporated into the analyzed material as well as biogenic changes due to the diagenesis process.

As a pioneering study on glyptodont carapace characterization, drawing parallels with modern relatives like armadillos helps shed light on the incorporation of various elements. A comparison between the modern armadillo and *Neosclerocalyptus* sp. armor reveals that both are primarily composed of hydroxyapatite, with collagen also present for

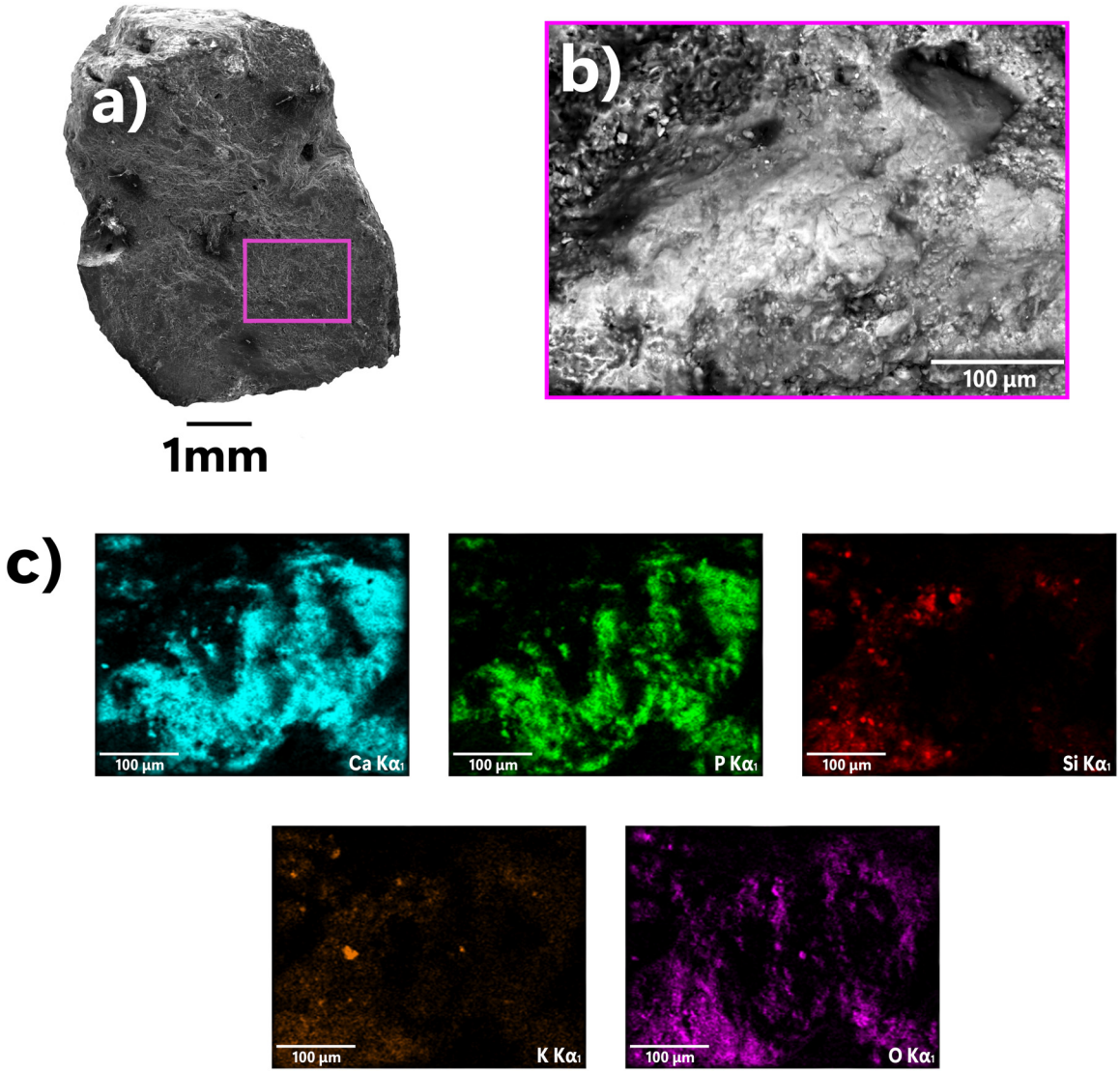

Figure 4. (a) Low magnification and recognition of the area for examination; (b) SEM image of the zone to analyze; (c) EDS elemental mapping analysis.

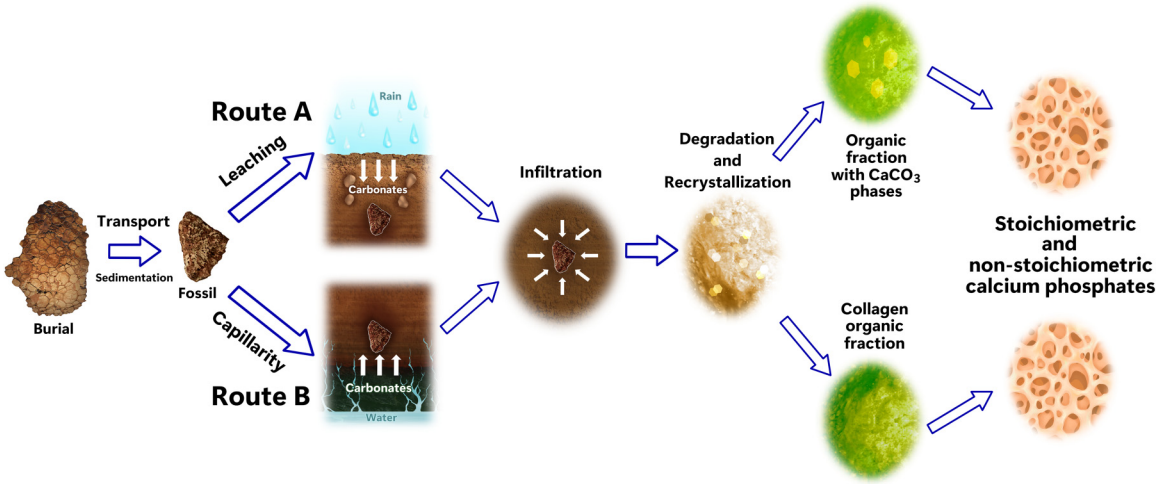

Figure 5. Model of possible diagenetic pathways according to the geological conditions of the fossil FACEN-PVert-0064.

this modern relative and potentially preserved in the case of the glyptodont carapace. The similarities in elemental composition and chemical structure suggest a shared fundamental framework, with any observed differences likely attributable to diagenetic processes during fossilization. The glyptodont osteoderms show evidence of mineralization influenced by elements such as Si, Ca, and Fe, which reflects postmortem alterations rather than intrinsic differences in their original composition. In contrast, the armadillo osteoderms retain their well-organized hydroxyapatite structure, reinforced by collagen fibers for flexibility.[77]

Similarly, concerning the morphological structure revealed through SEM analysis, the identified elements might be associated with enrichment or supergene processes subsequent to the burial of the material. Additionally, the fossil exhibits an amorphous and perforated surface, attributed to bioerosion and an extensive diagenesis process. It is plausible that these minerals constituted a significant component of the sedimentary layer at the extraction site of *Neosclerocalyptus* sp. in Neuland town, suggesting a combination of the apatitic nature of the osseous shell and silicates.

The identification of functional groups, crystalline phases, element characterization, morphological structure and knowledge of the extraction site of the fossil remains of the *Neosclerocalyptus* sp. suggest a possible diagenetic pathway. Considering the sedimentary rocks of the Paraguayan Chaco, the sediment can experience significant changes from the moment of deposition until its transformation into sedimentary rock.[78]

The theoretical process of fossilization explains how bone remains are preserved in sediments through permineralization, where water enriched with various compounds (Si, Fe, and Ca, among others) infiltrates and penetrate through the pores of the material, allowing for precipitation. This process strengthens the remains while preserving their original structure. Therefore, diagenesis is influenced by the characteristics of the sedimentary environment, which control the geochemical conditions during fossilization.[79–82] For the osteoderm under study in this manuscript, we have considered two possible diagenetic pathways A and B (Figure 5), inspired by the work of de Sousa et al.,[2] that could, to some extent, explain the process by which carbonate phases were incorporated into the osteoderm.

In the first pathway, Route A (leaching), moisture from the surface infiltrates through the soil, incorporating phases from carbonate-rich layers, such as calcite, which are pedogenetically incorporated in the more superficial layers. This process is influenced by relative humidity and biological activity, which facilitate the formation of pedogenic carbonates. Accumulation typically occurs in water-deficient areas, where climatic conditions favor carbonate precipitation.[83]

Route B (capillarity) suggests that carbonates form from deeper layers below the *Neosclerocalyptus* sp. site, unrelated to biological activity. Instead, this process is linked to water table fluctuations over long geological periods. The unsaturated zone above the phreatic level has negative pressure relative to local atmospheric pressure, causing moisture to rise via capillarity. Water molecules move upward due to surface tension and mineral attraction. When the capillary fringe reaches the evapotranspiration zone, up to about 375 m, depending on sediment, moisture loss leads to compound precipitation, enriching surface zones with materials from deeper layers.[84]

The incorporation of carbonate ions into the bone matrix is crucial for bone mineralization, particularly during recrystallization. During diagenesis, carbonate ions from surrounding sediments infiltrate the porous bone matrix, often substituting for phosphate groups in hydroxyapatite crystals. Osteoblasts transport calcium and phosphate into the extracellular matrix to form hydroxyapatite crystals. During recrystallization, carbonate ions help transform amorphous calcium phosphate into stable crystals, improving the resilience of the bone matrix. Carbonates influence hydroxyapatite's solubility, stability, and the pH needed for effective mineralization.[85–88]

The results indicate vibrational modes corresponding to carbonate groups, specifically large-sized crystal B-type carbonate, presumably formed by partial or total substitution of CO_3 for PO_4,[89,90] and the organic amide group, which may be responsible for the organic and collagen fractions. These processes possibly lead to the formation of both stoichiometric and non-stoichiometric calcium phosphates.

Finally, it is suggested that the recrystallization process may have begun in the early stages of diagenesis, and that during this process, up until late diagenesis, the total or partial incorporation of other trace elements identified in both the fossil and sediment may have occurred within the apatite structure of the fossil, influenced by the surrounding environmental conditions.[91,92]

Conclusion

Through FT-IR analyses, vibration modes corresponding to phosphate, carbonate, hydroxyl, carboxyl, methyl, and amide groups were identified, along with the presence of crystalline phases and various elements.

The GDM allowed for the identification of individual bands within overlapped vibration modes, providing detailed bond information. Additionally, diffraction patterns confirmed the crystallinity and apatitic nature of the samples, while fluorescence spectra assessed the integration of new elements. SEM-EDS analysis provided a microstructural display of the surface and examined the elements present.

Notably, the appearance of a new crystalline phase (quartz), along with changes in peak positions and FWHM values, indicated alterations in mineral purity and crystallinity due to environmental interactions. This suggests a diagenetic pathway involving initial amorphous development followed by exposure to calcium carbonate-rich water, leading to recrystallization of hydroxyapatite, filtration of calcite into pores, and the total or partial incorporation of other elements identified in both the fossil remains and the surrounding sediment.

Acknowledgments

This work was supported by the Consejo Nacional de Ciencia y Tecnología (CONACYT) of Paraguay, finance code PINV15-120. This research is part of the IAEA-funded Technical Cooperation Project: "Strengthening Capabilities for the Utilization of Nuclear and Radiation Technology to Characterize, Conserve, and Preserve Cultural Heritage," project code RLA1019. Thanks to the University Research Scholarship Program «Andrés Borgognon Montero» (PUBIABM) and Ganadera 13 de Mayo S.A., for the technical, scientific, and financial support in developing and concluding this study. Thanks to the Scientific Initiation Program (PIC) of FACEN–UNA for providing the necessary resources and infrastructure.

Declaration of Conflicting Interests

The authors declared no potential conflicts of interest with respect to the research, authorship, and/or publication of this article.

Funding

The authors received no financial support for the research, authorship, and/or publication of this article.

ORCID iDs

Deyne SM Buzarquis Arias https://orcid.org/0009-0000-0691-512X
Edher Herrera https://orcid.org/0000-0002-0629-202X
Christian F Colman https://orcid.org/0009-0001-1137-8290
Yennifer Sarubbi Jacks https://orcid.org/0009-0007-4901-4330
Sergio D Ríos https://orcid.org/0000-0002-0483-944X
Ricardo Souberlich https://orcid.org/0000-0001-6448-9835
Christian J Sánchez Gonzales https://orcid.org/0009-0008-4353-7875
Alex Matos da Silva Costa https://orcid.org/0000-0001-6942-8476

Supplemental Materials

All supplemental material mentioned in the text is available in the online version of the journal.

References

1. A. Gomes, B. Becker Kerber, G. Osés, G. Prado, et al. "Paleometry as a Key Tool to Deal with Paleobiological and Astrobiological Issues: Some Contributions and Reflections on the Brazilian Fossil Record". Int. J. Astrobiol. 2019. 18(6): 1–15. 10.1017/S1473550418000538
2. D.V. de Sousa, E. Eltink, R.A.P. Oliveira, J.F. Félix, L. M. Guimarães. "Diagenetic Processes in Quaternary Fossil Bones from Tropical Limestone Caves". Sci. Rep. 2020. 10(1): 21425. 10.1038/s41598-020-78482-0
3. N.T. Boaz, J. Hampel. "Strontium Content of Fossil Tooth Enamel and Diet of Early Hominids". J. Paleontol. 1978. 52(4): 928–933. https://www.jstor.org/stable/1303911
4. L.C. de Queiroz, T. Carlisbino, E.V.H. Agressott, A.R. Paschoal, et al. "Paleoenvironmental Interpretations of Irati and Mangrullo Formations (Permian of Paraná Basin) Based on Rocks and Fossil Bones Through Spectroscopy Techniques". Vib Spectrosc. 2020. 110: 103110. 10.1016/j.vibspec.2020.103110
5. A.O. Delgado, P.V. Buck, G.L. Osés, R.P. Ghilardi, et al. "Paleometry: A Brand New Area in Brazilian Science". Mat Res. 2014. 17(6): 1434–1441. 10.1590/1516-1439.288514
6. D.J. Peppe, A. Baumgartner, A. Flynn, B. Blonder. "Reconstructing Paleoclimate and Paleoecology Using Fossil Leaves". In: D.A. Croft, D.F. Su, S.W. Simpson, editors. Methods in Paleoecology: Reconstructing Cenozoic Terrestrial Environments and Ecological Communities. Cham, Switzerland: Springer, 2018. Pp. 289–317.
7. G. Falgayrac, R. Vitale, Y. Delannoy, H. Behal, et al. "Bone Molecular Modifications Induced by Diagenesis Followed-Up for 12 Months". Biology (Basel). 2022. 11(10): 1542. 10.3390/biology11101542
8. J.R. Rengger. Reise nach Paraguay in den Jahren 1818 bis 1826. Aarau: Saeurlaender, 1835.
9. J. Pasteris, B. Wopenka, E. Valsami-Jones. "Bone and Tooth Mineralization: Why Apatite?". Elements. 2008. 4(2): 97–104. 10.2113/GSELEMENTS.4.2.97

10. T. Kallaste, J. Nemliher. "Apatite Varieties in Extant and Fossil Vertebrate Mineralized Tissues". J. Appl. Crystallogr. 2005. 38 (4): 587–594. 10.1107/S0021889805011404
11. S. Von Euw, Y. Wang, G. Laurent, C. Drouet, et al. "Bone Mineral: New Insights into Its Chemical Composition". Sci. Rep. 2019. 9: 8456. 10.1038/s41598-019-44620-6
12. P.W. Brown, B. Constantz. Hydroxyapatite and Related Materials. Boca Raton, Florida: CRC Press, 2017.
13. G. de la Puerta. Química Orgánica General y Aplicada a la Farmacia, Medicina, Industria, Agricultura y Artes. Galiciana: Imp. de T. Fortanet, 1872.
14. Y. Asscher, L. Regev, S. Weiner, E. Boaretto. "Atomic Disorder in Fossil Tooth and Bone Mineral: An FT-IR Study Using the Grinding Curve Method". Archeo Sci Revue d'Archéométrie. 2011. 35: 135–141. 10.4000/archeosciences.3062
15. J. Anné, R.A. Wogelius, N.P. Edwards, A. Van Veelen, et al. "Chemistry of Bone Remodelling Preserved in Extant and Fossil Sirenia". Metallomics. 2016. 8(5): 508–513. 10.1039/c5mt00311c
16. Newesely H. "Fossil Bone Apatite". Appl. Geochem. 1989. 4(3): 233–245. 10.1016/0883-2927(89)90023-1
17. A. Sillen. "Diagenesis of the Inorganic Phase of Cortical Bone". In: T.D. Price, editor. The Chemistry of Prehistoric Human Bone. Cambridge: University of Cambridge Press, 1989. Pp. 221–229.
18. D.B. Thomas, C.M. McGoverin, R.E. Fordyce, R.D. Frew, K. C. Gordon. "Raman Spectroscopy of Fossil Bioapatite: A Proxy for Diagenetic Alteration of the Oxygen Isotope Composition". Palaeogeogr, Palaeoclimatol, Palaeoecol. 2011. 310(1–2): 62–70. 10.1016/j.palaeo.2011.06.016
19. Y.C. Lee, C.C. Chiang, P.Y. Huang, C.Y. Chung, et al. "Evidence of Preserved Collagen in an Early Jurassic Sauropodomorph Dinosaur Revealed by Synchrotron FT-IR Microspectroscopy". Nat. Commun. 2017. 8(1): 14220. 10.1038/ncomms14220
20. E.T. Saitta, R. Liang, M.C. Lau, C.M. Brown, et al. "Cretaceous Dinosaur Bone Contains Recent Organic Material and Provides an Environment Conducive to Microbial Communities". Elife. 8: e46205. 10.7554/eLife.46205
21. E.D. Cafaro, E.M. Latrubesse, C.G. Ramonell. "Distribución Espacial de Patrones de Cauce en Abanicos Aluviales Chaqueños". Cuarto Simposio Regional Sobre Hidráulica de Ríos. 2009. 9–10.
22. C.E. Uba, C. Heubeck, C. Hulka. "Evolution of the Late Cenozoic Chaco Foreland Basin, Southern Bolivia". Basin Res. 2006. 18(2): 145–70. 10.1111/j.1365-2117.2006.00291.x
23. C.E. Uba, C. Heubeck, C. Hulka. "Facies Analysis and Basin Architecture of the Neogene Subandean Synorogenic Wedge, Southern Bolivia". Sediment Geol. 2005. 180(3–4): 91–123. 10.1016/j.sedgeo.2005.06.013
24. M. Iriondo. "Geomorphology and Late Quaternary of the Chaco (South America)". Geomorphology. 1993. 7(4): 289–303. 10.1016/0169-555X(93)90059-B
25. W. Kruck, F. Helms, M. Geyh, J. Suriano, et al. "Late Pleistocene–Holocene History of Chaco–Pampa Sediments in Argentina and Paraguay". Quat. Sci. J. 2011. 60(1): 188–202. 10.3285/eg.60.1.13
26. E.M. Latrubesse, J. Stevaux, E. Cremon, J.H. May, et al. "Late Quaternary Megafans, Fans, and Fluvio–Aeolian Interactions in the Bolivian Chaco, Tropical South America". Palaeogeogr, Palaeoclimatol, Palaeoecol. 2012. 356–357: 75–88. 10.1016/j.palaeo.2012.04.003
27. E.M. Latrubesse. "Large Rivers, Megafans and Other Quaternary Avulsive Fluvial Systems: A Potential 'Who's Who' in the Geological Record". Earth Sci. Rev. 2015. 146: 1–30. 10.1016/j.earscirev.2015.03.004
28. J.P. Martín-Vide, M. Amarilla, F.J. Zárate. "Collapse of the Pilcomayo River". Geomorphology. 2014. 205: 155–163. 10.1016/j.geomorph.2012.12.007
29. J.H. May, J. Argollo, H. Veit. "Holocene Landscape Evolution along the Andean Piedmont, Bolivian Chaco". Palaeogeogr, Palaeoclimatol, Palaeoecol. 2008. 260(3–4): 505–520. 10.1016/j.palaeo.2007.12.009
30. M.M. McGlue, P.H. Smith, H. Zani, A. Silva, et al. "An Integrated Sedimentary Systems Analysis of the Río Bermejo (Argentina): Megafauna Character in the Overfilled Southern Chaco Foreland Basin". J. Sediment. Res. 2016. 86(12): 1359–1377. 10.2110/jsr.2016.82
31. G.H. Sambrook Smith, J.L. Best, J.Z. LeRoy, O. Orfeo. "The Alluvial Architecture of a Suspended Sediment Dominated Meandering River: The Río Bermejo, Argentina". Sedimentology. 2015. 63(5): 1187–1208. 10.1111/sed.12256
32. P.A. Suárez, M.C. Sartirana, O. Orfeo. "Caracteres Sedimentológicos de Ambientes Fluviales de La Llanura Subtropical Chaqueña (Argentina)". Acta Geológica Lilloana. 2010. 22(1–2): 34–45.
33. M. Thalmeier, D. Kröhling, E. Brunetto. "The Geomorphology and Late Quaternary Sedimentary Record of the Salado/Juramento Fluvial Megafan, Central Andes Foreland Basin (Chaco Plain, Argentina)". Geomorphology. 2020. 373: 107495. 10.1016/j.geomorph.2020.107495
34. C.A.C. Kuhn. The Geological Evolution of the Paraguayan Chaco. [Doctor of Philosophy in Geoscience Dissertation]. Lubbock, Texas: Texas Tech University, 1991.
35. J. Argollo Bautista, M.H. Iriondo. El Cuaternario de Bolivia y Regiones Vecinas. Santa Fe: Museo Provincial de Ciencias Naturales Florentino Ameghino, 2017.
36. E.B. Eckel. Geology and Mineral Resources of Paraguay: A Reconnaissance. Washington, DC: U.S. Department of the Interior, U.S. Government Printing Office, 1959.
37. Government of Paraguay. Hallan fósil de más de 9 mil años en Presidente Hayes.2020. https://cultura.gov.py/2020/08/hallan-fosil-de-mas-de-9-mil-anos-en-presidente-hayes/ [accessed Feb 27 2025].
38. Zurita A.E., G.J. Scillato, A.A. Carlini. "Paleozoogeographic, Biostratigraphic, and Systematic Aspects of the Genus *Sclerocalyptus* Ameghino, 1891 (Xenarthra, Glyptodontidae) of Argentina". 2005. 20(1–2): 121–129. 10.1016/j.jsames.2005.06.013
39. A.E. Zurita. Sistemática y Evolución de los Hoplophorini (Xenarthra: Glyptodontidae: Hoplophorinae. Mioceno Tardío-Holoceno Temprano. [Doctoral Thesis]. Argentina: Universidad Nacional de La Plata, 2007.
40. S.I. Quiñones, M. De los Reyes, A.E. Zurita, F. Cuadrelli, et al. "*Neosclerocalyptus* Paula Couto (Xenarthra, Glyptodontidae) in the Late Pliocene–Earliest Pleistocene of the Pampean Region (Argentina): Its Contribution to the Understanding of Evolutionary History of Pleistocene Glyptodonts". J. South Am. Earth Sci. 2020. 103: 102701. 10.1016/j.jsames.2020.102701
41. A.E. Zurita, A. Scarano, A. Carlini, G.J. Scillato-Yané, E. Soibelzon. "*Neosclerocalyptus* spp. (Cingulata: Glyptodontidae: Hoplophorini): Cranial Morphology and Palaeoenvironments Along the

Changing Quaternary". J. Nat. History. 2011. 45(15–16): 893–914. 10.1080/00222933.2010.536917
42. N. Pleshko, A. Boskey, R. Mendelsohn. "Novel Infrared Spectroscopic Method for the Determination of Crystallinity of Hydroxyapatite Minerals". Biophys. J. 1991. 60(4): 786–793. 10.1016/S0006-3495(91)82113-0
43. B.H. Stuart. Infrared Spectroscopy: Fundamentals and Applications. Chichester, UK: J. Wiley, 2004.
44. F. Menges. "Spectragryph: Optical Spectroscopy Software". Spectroscopy. 2024. https://www.effemm2.de/spectragryph/index.html
45. A. Brangule, K. Gross. "Importance of FT-IR Spectra Deconvolution for the Analysis of Amorphous Calcium Phosphates". IOP Conf Ser: Mater. Sci. Eng. 2015. 77: 012027. 10.1088/1757-899X/77/1/012027
46. C. Rey, M. Shimizu, B. Collins, M.J. Glimcher. "Resolution-Enhanced Fourier Transform Infrared Spectroscopy Study of the Environment of Phosphate Ion in the Early Deposits of a Solid Phase of Calcium Phosphate in Bone and Enamel and their Evolution with Age: 2. Investigations in the v3 PO_4 Domain". Calcif. Tissue Int. 1991. 49(6): 383–388. 10.1007/BF02555847
47. I.E. Boldeskul, L.F. Sukhodub, A.N. Kalinkevich, V. D. Khavryutchenko. "Ab Initio Modelling of Calcium Phosphate Clusters and Their Vibrational Spectra". Cond. Matter Phys. 2006. 9(4): 669–679. 10.5488/CMP.9.4.669
48. M. Wojdyr. "Fityk: A General-Purpose Peak Fitting Program". J. Appl. Crystallogr. 2010. 43(5–1): 1126–1128. 10.1107/S0021889810030499
49. G. Britton, S. Liaaen-Jensen, H. Pfander. Carotenoids. Basel: Springer AG, 2008.
50. S. Koutsopoulos. "Synthesis and Characterization of Hydroxyapatite Crystals: A Review Study on the Analytical Methods". J. Biomed. Mater. Res. 2002. 62(4): 600–612. 10.1002/jbm.10280
51. S.J. Joris, C.H. Amberg. "The Nature of Deficiency in Nonstoichiometric Hydroxyapatites. II. Spectroscopic Studies of Calcium and Strontium Hydroxyapatites". J. Phys. Chem. 1971. 75(20): 3172–3178. 10.1021/j100689a025
52. E.P. Paschalis, E. DiCarlo, F. Betts, P. Sherman, et al. "FT-IR Microspectroscopic Analysis of Human Osteonal Bone". Calcif Tissue Int. 1996. 59(6): 480–487. 10.1007/BF00369214
53. E. Herrera, S. Ríos, C. Aquino, C. Colman, et al. "Characterization of Dental Fragments of *Toxodon* sp. (Mammalia, Notoungulata) by Multiple Physical and Chemical Techniques". Vib Spectrosc. 2021. 114: 103248. 10.1016/j.vibspec.2021.103248
54. A. Antonakos, E. Liarokapis, T. Leventouri. "Micro-Raman and FT-IR Studies of Synthetic and Natural Apatites". Biomaterials. 2007. 28(19): 3043–3054. 10.1016/j.biomaterials.2007.02.028
55. B.O. Fowler. "Infrared Studies of Apatites. I. Vibrational Assignments for Calcium, Strontium, and Barium Hydroxyapatites Utilizing Isotopic Substitution". Inorg. Chem. 1974. 13(1): 194–207. 10.1021/ic50131a039
56. A.P. Mamede, D. Gonçalves, M.P.M. Marques, L.A.E. Batista de Carvalho. "Burned Bones Tell Their Own Stories: A Review of Methodological Approaches to Assess Heat-Induced Diagenesis". Appl. Spectrosc. Rev. 2018. 53(8): 603–635. 10.1080/05704928.2017.1400442
57. G. Piga, A. Santos-Cubedo, S. Moya Solà, A. Brunetti, et al. "An X-Ray Diffraction (XRD) and X-Ray Fluorescence (XRF) Investigation in Human and Animal Fossil Bones from Holocene to Middle Triassic". J. Archaeol. Sci. 2009. 36(9): 1857–1868. 10.1016/j.jas.2009.04.013
58. L.E. Wright, H.P. Schwarcz. "Infrared and Isotopic Evidence for Diagenesis of Bone Apatite at Dos Pilas, Guatemala: Palaeodietary Implications". J. Archaeol. Sci. 1996. 23(6): 933–944. 10.1006/jasc.1996.0087
59. D. Eichert, C. Drouet, H. Sfihi. "Nanocrystalline Apatite Based Biomaterials: Synthesis, Processing, and Characterization". In: J. B. Kendall, editor. Biomaterials Research Advances. New York: Nova Science Publishers, 2008. Pp. 93–143.
60. M.M. Beasley, E.J. Bartelink, L. Taylor, R.M. Miller. "Comparison of Transmission FT-IR, ATR, and DRIFT Spectra: Implications for Assessment of Bone Bioapatite Diagenesis". J. Archaeol. Sci. 2014. 46: 16–22. 10.1016/j.jas.2014.03.008
61. G. Barraza-Garza, L.A. de la Rosa, A. Martínez-Martínez, H. Castillo-Michel, et al. "La Microespectroscopía de Infrarrojo con Transformada de Fourier (FT-IRM) en El Estudio de Sistemas Biológicos". Rev Latinoam de Quimica. 2013. 41(3): 125–148.
62. C. Chadefaux, A.S. Le Hô, L. Bellot-Gurlet, I. Reiche. "Curve-Fitting Micro-ATR-FT-IR Studies of the Amide I and II Bands of Type I Collagen in Archaeological Bone Materials". e-Preserv Sci 2009. 6: 129–137.
63. G. Rytwo, R. Zakai, B. Wicklein. "The Use of ATR-FT-IR Spectroscopy for Quantification of Adsorbed Compounds". J. Spectrosc. 2015. 1: 1–8. 10.1155/2015/727595
64. A. Olcott Marshall, C.P. Marshall. "Vibrational Spectroscopy of Fossils". Palaeontology. 2015. 58(2): 201–211. 10.1111/pala.12144
65. A.C. Chapman, D.A. Long, D.T.L. Jones. "Spectra of Phosphorous Compounds: II. The Force Constants of Orthophosphates". Spectrochim. Acta. 1965. 21(4): 633–640. 10.1016/0371-1951(65)80019-4
66. E.P. Paschalis, R. Mendelsohn, A.L. Boskey. "Infrared Assessment of Bone Quality: A Review". Clin Orthop Relat Res. 2011. 469(8): 2170–2178. 10.1007/s11999-010-1751-4
67. J.C. Elliott, R. Wilson, S.E.P. Dowker. "Apatite Structures". Adv. X-ray Anal. 2002. 45: 172–181.
68. M.E. Fleet, X. Liu, P.L. King. "Accommodation of the Carbonate Ion in Apatite: An FTIR and X-Ray Structure Study of Crystals Synthesized at 2–4 GPa". Am. Mineral. 2004. 89(10): 1422–1432. 10.2138/am-2004-1009/html
69. Z. Jurašeková, G. Fabriciová, L.F. Silveira, Y.N. Lee, et al. "Raman Spectra and Ancient Life: Vibrational ID Profiles of Fossilized (Bone) Tissues". Int. J. Mol. Sci. 2022. 23(18): 10689. 10.3390/ijms231810689
70. C. Otto, C.J. de Grauw, J.J. Duindam, N.M. Sijtsema, J. Greve. "Applications of Micro-Raman Imaging in Biomedical Research". J. Raman. Spectrosc. 1997. 28(2–3): 143–150. 10.1002/%28SICI%291097-4555%28199702%2928%3A2/3%3C143%3A%3AAID-JRS70%3E3.0.CO%3B2-9
71. R.J. Merriman, M. Frey. "Patterns of Very Low-Grade Metamorphism in Metapelitic Rocks. En: Low-Grade Metamorphism". In: M. Frey, D. Robinson, editors. Low-Grade Metomorphism. Chichester, UK: John Wiley and Sons, Ltd., 1998. Pp. 61–107.
72. S. Armengol, C. Ayora, M. Manzano, S.A. Bea, S. Martínez. "The Role of Loess Weathering in the Groundwater Chemistry of the

Chaco–Pampean Plain (Argentina)". J. Hydrol. 2020. 587: 124984. 10.1016/j.jhydrol.2020.124984

73. M.T. Krajcarz. "Alteration of the Metal Content in Animal Bones after 2.5-Year Experimental Exposure to Sediments". Archaeol. Anthropol. Sci. 2019. 11(1): 361–372. 10.1007/s12520-017-0533-2
74. F. Tanjin, M.M. Rahman, Y.N. Jolly, K.K. Riya, et al. "Accumulation and Phytoremediation Potentiality of Trace and Heavy Metals in Some Selected Aquatic Plants from a Highly Urbanized Subtropical Estuary". J. Marine Sci Eng. 2024. 12(7): 1131. 10.3390/jmse12071131
75. R.F. Ediagbonya, O.T. Balogun. "Potential Risk Assessment and Spatial Distribution of Elemental Concentrations in Sediment". Appl. Water Sci. 2020. 10(7): 176. 10.1007/s13201-020-01260-w
76. Z. García-López, A.M. Cortizas, N. Álvarez-Fernández, O. López-Costas. "Understanding Necrosol Pedogenetical Processes in Post-Roman Burials Developed on Dunes Sands". Sci. Rep. 2022. 12(1): 10619. 10.1038/s41598-022-14750-5
77. I.H. Chen, J.H. Kiang, V. Correa, M.I. Lopez, et al. "Armadillo Armor: Mechanical Testing and Micro-Structural Evaluation". J. Mech. Behav. Biomed. Mater. 2011. 4(5): 713–722. 10.1016/j.jmbbm.2010.12.013
78. E.J. Tarbuck, F.K. Lutgens. Ciencias de la Tierra: Una Introducción a la Geología Física. Madrid: Pearson Educación, 2005.
79. E.L. Mayer, A. Hubbe, J. Botha-Brink, A.M. Ribeiro, et al. "Diagenetic Changes on Bone Histology of Quaternary Mammals from a Tropical Cave Deposit in Southeastern Brazil". Palaeogeogr, Palaeoclimatol, Palaeoecol. 2020. 537: 109372. 10.1016/j.palaeo.2019.109372
80. C.M. Nielsen-Marsh, R.E.M. Hedges. "Patterns of Diagenesis in Bone I: The Effects of Site Environments". J. Archaeol. Sci. 2000. 27(12): 1139–1150. 10.1006/jasc.1999.0537
81. R.E.M. Hedges, A.R. Millard. "Bones and Groundwater: Towards the Modelling of Diagenetic Processes". J. Archaeol. Sci. Rep. 1995. 22(2): 155–164. 10.1006/jasc.1995.0017
82. E.T. Saitta, T.G. Kaye, J. Vinther. "Sediment-Encased Maturation: A Novel Method for Simulating Diagenesis in Organic Fossil Preservation". Palaeontology. 2019. 62(1): 135–150. 10.1111/pala.12386
83. R. Ovalle, O. Seguel, M. Pfeiffer. "Genesis y Ocurrencia de Carbonatos en los Suelos". Agro. Sur. 2023. 51(1): 1–17. 10.4206/agrosur.2023.v51n1-01
84. J.L. Keeling. "Metal Ion Dispersion Through Transported Cover at Moonta, South Australia". In: Proceedings of the CRC LEME Regional Regolith Symposia. Adelaide, Australia. 10–26 November 2004. Pp. 161–165.
85. F. Berna, A. Matthews, S. Weiner. "Solubilities of Bone Mineral from Archaeological Sites: The Recrystallization Window". J. Archaeol. Sci. 2004. 31(7): 867–882. 10.1016/j.jas.2003.12.003
86. P.H. Schlesinger, H.C. Blair, D.B. Stolz, V. Riazanski, et al. "Cellular and Extracellular Matrix of Bone, with Principles of Synthesis and Dependency of Mineral Deposition on Cell Membrane Transport". Am. J. Physiol. Cell Physiol. 2019. 318 (1): C111–C124. 10.1152/ajpcell.00120.2019
87. V. Šromová, D. Sobola, P. Kaspar. "A Brief Review of Bone Cell Function and Importance". Cells. 2023. 12(21): 2576. 10.3390/cells12212576
88. X. Feng. "Chemical and Biochemical Basis of Cell–Bone Matrix Interaction in Health and Disease". Curr Chem Biol. 2009. 3(2): 189–196. 10.2174/187231309788166398
89. F. Ren, Y. Leng. "Carbonated Apatite, Type-A or Type-B?". Key Eng. Mater. 2011. 493–494: 293–297. 10.4028/www.scientific.net/KEM.493-494.293
90. M.E. Fleet, X. Liu. "Coupled Substitution of Type A and B Carbonate in Sodium-Bearing Apatite". Biomaterials. 2007. 28 (6): 916–926. 10.1016/j.biomaterials.2006.11.003
91. P. Gueriau, C. Jauvion, C. Mocuta. "Show Me Your Yttrium, and I Will Tell You Who You Are: Implications for Fossil Imaging". Palaeontology. 2018. 61(6): 981–990. 10.1111/pala.12377
92. I. Marchetti, F. Ricardi-Branco, F. Callefo, R. Delcourt, et al. "Fossil Diagenesis and Ontogenetic Insights of Crocodyliform Bones from the Adamantina Formation, Bauru Basin, Brazil". J. South Am. Earth Sci. 2019. 96: 102327. 10.1016/j.jsames.2019.102327